Research Article Vol. 13, No. 3 / 1 Mar 2022 / Biomedical Optics Express 1497
Biomedical Optics EXPRESS

Handheld laser scanning microscope catheter for real-time and *in vivo* confocal microscopy using a high definition high frame rate Lissajous MEMS mirror

JAEHUN JEON,[1,2] HYUNWOO KIM,[1,2] HYUNWOO JANG,[1] KYUNGMIN HWANG,[3] KYUYOUNG KIM,[3] YOUNG-GYUN PARK,[1] AND KI-HUN JEONG[1,2,*]

[1] *Department of Bio and Brain Engineering, Korea Advanced Institute of Science and Technology (KAIST), 291 Daehak-ro, Yuseong-gu, Daejeon 34141, Republic of Korea*
[2] *KAIST Institute for Health Science and Technology (KIHST), KAIST, 291 Daehak-ro, Yuseong-gu, Daejeon, 305-701, Republic of Korea*
[3] *VPIX Medical, Inc, Deajeon, 34873, Republic of Korea*
[*] *kjeong@kaist.ac.kr*

Abstract: A handheld confocal microscope using a rapid MEMS scanning mirror facilitates real-time optical biopsy for simple cancer diagnosis. Here we report a handheld confocal microscope catheter using high definition and high frame rate (HDHF) Lissajous scanning MEMS mirror. The broad resonant frequency region of the fast axis on the MEMS mirror with a low Q-factor facilitates the flexible selection of scanning frequencies. HDHF Lissajous scanning was achieved by selecting the scanning frequencies with high greatest common divisor (GCD) and high total lobe number. The MEMS mirror was fully packaged into a handheld configuration, which was coupled to a home-built confocal imaging system. The confocal microscope catheter allows fluorescence imaging of *in vivo* and *ex vivo* mouse tissues with 30 Hz frame rate and 95.4% fill factor at 256×256 pixels image, where the lateral resolution is 4.35 μm and the field-of-view (FOV) is 330 $\mu m \times 330$ μm. This compact confocal microscope can provide diverse handheld microscopic applications for real-time, on-demand, and *in vivo* optical biopsy.

1. Introduction

In vivo optical biopsy facilitates rapid and simple cancer diagnosis. Conventional biopsy and histopathology require complex and time-consuming sample preparation such as fixation, embedding, sectioning, and staining [1]. The optical biopsy without sample preparation exhibits considerable strength in shortening conventional time-consuming tasks [2] and facilitating cancer resection with minimal tissue removal under immediate feedback. However, the physical volume of conventional laser scanning microscopes significantly restricts diverse handheld applications for optical biopsy [3]. In addition, periodic and random motion artifacts often impede accurate diagnosis due to the substantial reduction of imaging quality [4]. Therefore, the development of high-speed imaging systems inside a compact microscope is still challenging for precise *in vivo* optical biopsy.

MEMS (Micro Electro Mechanical Systems) scanners such as scanning lenses [5], scanning mirrors [6–9], or scanning fibers [10–12] have been actively applied for compact and rapid laser scanning microscopes. They effectively downsize the scanning microscope by substituting a bulky scanning unit and still maintain high performance [13]. For instance, the handheld dual-axis [14] and line-scanned [15,16] confocal microscopes improve the axial resolution and the frame rate, respectively. In addition, Lissajous scanning, which exhibits bi-axial rapid resonant scanning, was also utilized for high frame rate scanning [17,18]. Unlike raster scanning, Lissajous scanning

#447558 https://doi.org/10.1364/BOE.447558
Journal © 2022 Received 3 Nov 2021; revised 9 Feb 2022; accepted 9 Feb 2022; published 15 Feb 2022

Biomedical Optics EXPRESS

has many benefits in high mechanical stability and a low voltage operation [17], even though it exists a trade-off between the frame rate and the fill factor. The selection rule of scanning frequencies for high definition and high frame rate (HDHF) Lissajous scanning overcomes the trade-off relation [19]. The selection rule was recently applied to electrostatic Lissajous scanning MEMS mirrors with a low Q-factor for high definition and high frame rate imaging [20]. These HDHF Lissajous scanning MEMS mirrors can be applied to high-quality real-time and *in vivo* imaging.

Here we report a handheld microscope catheter for real-time and *in vivo* confocal imaging applications using HDHF Lissajous scanning MEMS mirror. Figure 1 shows the schematic illustration for the handheld confocal microscopic module based on Lissajous scanning MEMS mirror. The module consists of collimation and reflection optics, MEMS mirror, and a GRIN lens. The resonantly scanning electrostatic MEMS mirror has an inner mirror and a surrounding frame mirror for Lissajous scanning. The MEMS mirror allows HDHF Lissajous scanning by selecting the scanning frequencies near the resonance within the resonant bandwidth, which are indicated by the color box. The inner mirror has a low Q-factor, which provides broadband of resonant frequency for the flexible selection of scanning frequency. The selected frequencies have high greatest common divisor (GCD) and high total lobe number in the Lissajous curve, i.e., the sum of two scanning frequencies divided by their GCD. They allow HDHF Lissajous scanning with over 30 Hz frame rate and over 95.4% fill factor at 256×256 pixels image.

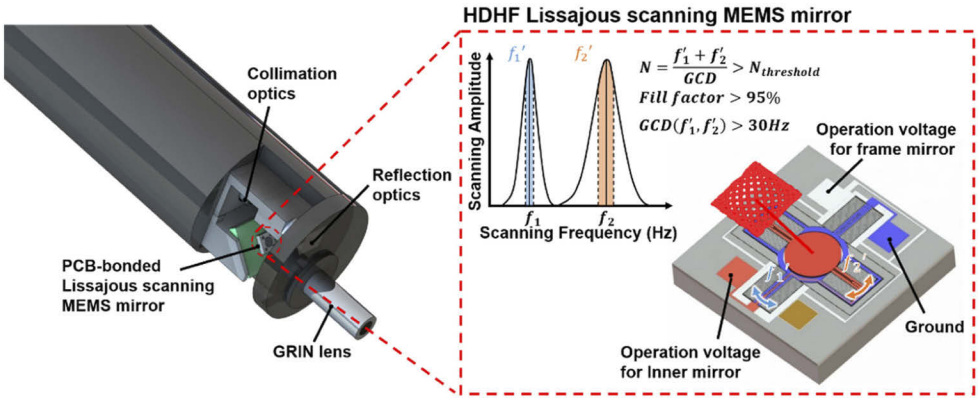

Fig. 1. A schematic illustration for the handheld confocal microscope catheter using Lissajous scanning MEMS mirror. The module consists of collimation and reflection optics, MEMS mirror, and a GRIN lens. The MEMS mirror facilitates HDHF Lissajous scanning by selecting the scanning frequencies near the resonant frequency within the resonant bandwidth, which are indicated by the colored region. The inner mirror has a low Q-factor to provide a board resonant frequency band for flexible frequency selection. The selection of scanning frequencies with high GCD and high total lobe number realizes HDHF Lissajous scanning with over 30 Hz frame rate and over 95.4% fill factor at 256×256 pixels image.

2. Result and discussion

2.1. HDHF Lissajous scanning MEMS mirror

The MEMS mirror was designed to perform HDHF Lissajous scanning. The frame rate linearly increases with the GCD of bi-axial scanning frequencies and the fill factor monotonically increases with the total lobe number of the Lissajous pattern [19]. Based on the frequency selection rule, the biaxial scanning frequencies require a total lobe number over 358 and GCD over 30 to reach the target fill factor over 95% and frame rate over 30 Hz at 256×256 pixels image. As a result, the

Biomedical Optics EXPRESS

sum of resonant frequencies from two axes is set to over 10,740 Hz for HDHF Lissajous scanning. In addition, the inner mirror was designed to have a low Q-factor for flexible frequency selection by providing a wide resonant band. The resonant frequency and Q-factor were determined by the physical dimension of mirror and torsional bar. For a particular case, the diameter of the MEMS mirror was set to 500 μm for obtaining high scanning frequency over 5 kHz in a small volume and all the individual parameters related to the resonant frequency were determined by using the finite element analysis (FEM, COMSOL Multi-physics ver. 5.4). In addition, the Q-factor was controlled by the width of the torsional bar [21].

The Lissajous scanning MEMS mirror was fabricated on a 6-inch SOI wafer (silicon-on-insulator wafer, top Si: 30μm, buried oxide layer: 2μm, bottom Si: 400μm). Figure 2(a) describes the microfabrication procedures of MEMS mirror. First, the silicon trench was defined on the top Silicon by using deep reactive ion etching (DRIE). Silicon dioxide was refilled for electrical isolation with wet oxidation and polysilicon was deposited for a physical connection between the inner and the frame mirrors via low-pressure chemical vapor deposition (LPCVD), respectively. Polysilicon and silicon dioxide on the front side were completely removed by using DRIE and wet etching, respectively. A 1,000 Å-thick aluminum film was thermally evaporated and defined in wet etching. Microstructures such as comb-drives, mirror frame, and torsional bar were defined by using DRIE. The backside was finally opened by using DRIE and the buried oxide layer was etched in buffered oxide etchant (BOE) to release the MEMS mirror. The individual MEMS mirror was released from the wafer by using the fused-tether method with the Y-shape tethers [22]. Figure 2(b) shows the top SEM image of the microfabricated device. The footprint of the MEMS mirror is $1.68 \times 1.8 \times 0.43\ mm^3$. In addition, the thin torsional bar of the inner mirror (right bottom of Fig. 2(b)) induces a low Q-factor [21] and low resonant frequency and vice versa in the frame mirror (right top in Fig. 2(b)). Figure 2(c) shows the frequency response of frame and inner mirrors at applied voltages of 34 V_{pp} and 22 V_{pp}, respectively. The MEMS mirror shows nonlinear resonance, previously reported in the parametric resonant MEMS mirror [23] and thus the frequency response is measured at the up-sweeping condition for operation without frequency sweeping. The frame and the inner mirrors have resonant frequencies at 5,038 Hz and 6,665 Hz, respectively. The inner mirror has a low Q-factor ($Q = 60.5$) ($Q = f_r / \Delta f_{FWHM}$, where f_r is the resonant frequency and Δf_{FWHM} is the full width at half maximum) for the flexible selection of scanning frequencies.

The MEMS scanner performs HDHF Lissajous scanning by applying the frequency selection rule. The scanning frequencies were selected within the following resonant frequency ranges: 5,038 Hz - 5,043 Hz for the frame mirror and 6,665 Hz - 6,715 Hz for the inner mirror. Figure 3(a) shows the color maps of the GCD (top) and total lobe number (bottom) for selecting the scanning frequency along with the biaxial frequency domain. The scanning frequencies corresponding to over both the GCD of 30 and the total lobe numbers of 358 are selected for 30 Hz frame rate and over 95% fill factor in 256×256 pixels. The selected frequencies are 5,040 Hz and 6,690 Hz, respectively and displayed in a dotted red box. The GCD and the total lobe number of selected frequencies are 30 and 391, respectively. Figure 3(b) shows the calculated scanning trajectories at 256×256 pixels image (top) and the optical images of scanning patterns (bottom) for the selected frequency set. The Lissajous pattern fills an image plane along the scanning time and the scanning pattern becomes saturated after the scanning time above the inverse of frame rate (1/30 s). Figure 3(c) shows the calculated fill factor along the scanning time at different pixel resolutions with a sampling rate of 8 MHz condition. The calculated fill factors are an average value for 200 different random phase conditions by considering the phase delay between the driving signals and the mirror motion. The selected frequency set provides HDHF Lissajous scanning with 95.4% fill factor at 1/30 s in 256×256 pixels.

Biomedical Optics EXPRESS

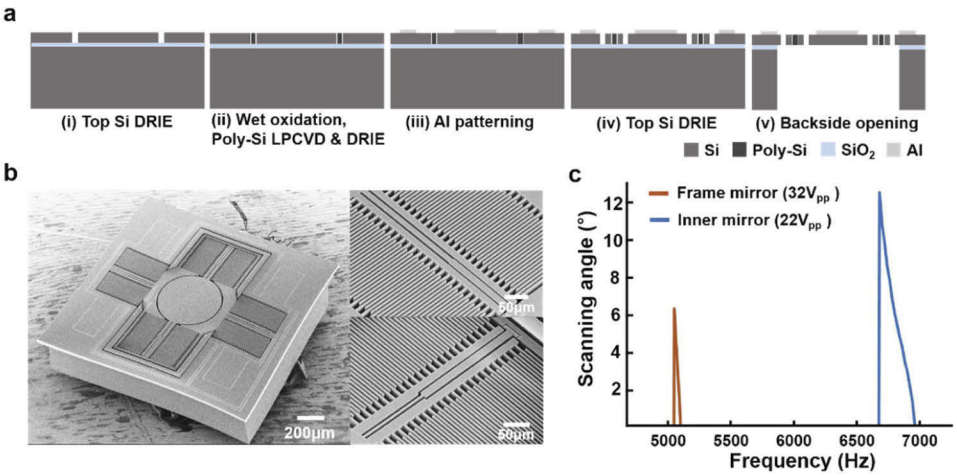

Fig. 2. a) Microfabrication procedure of Lissajous scanning MEMS mirror. b) SEM images of microfabricated MEMS mirror (left) and the flexures of frame mirror (right top) and inner mirror (right bottom). The footprint size of the MEMS mirror is $1.6 \times 1.8 \times 0.43\ mm^3$. c) Scanning frequency responses of the frame and inner mirrors at up-sweeping condition. The frame and the inner mirror have resonant frequencies at 5,038 Hz and 6,665 Hz, respectively. The inner mirror has a low Q-factor (Q = 60.5) to provide a broad-band resonant frequency for the flexible selection of scanning frequency.

2.2. *Packaging of the handheld confocal microscope catheter*

The compact microscope catheter consists of collimation and reflection optics, the MEMS mirror, and a GRIN lens. The microscope catheter uses a 785 nm laser as a light source. A single-mode fiber collimator (50-780-FC, Thorlabs) and right-angle mirror (No. 49405, Edmund optics) collimate a laser beam onto the MEMS scanner. The scanned light passes the commercial GRIN lens (No. 64526, Edmund optics) for beam focusing. Figure 4(a) shows the spot diagrams at the center and the scanning amplitude of 200 μm on the focal plane by using the ray tracing in ZEMAX. The distance between the GRINS lens and the MEMS mirror is set to provide the minimum RMS beam diameter at the periphery of the focal plane. The RMS beam diameters are less than 0.8 μm at the center and the edge. The individual optical components are precisely aligned with 3D printed jigs and anodized aluminum housing and then permanently glued with UV-curing epoxy. Figure 4(b) shows the beam profile for the fully packaged microscope catheter, measured by using the optical sectioning along the z-axis with a conventional confocal laser scanning microscope (LSM 510/CF26, Carl Zeiss). The working distance is about 190 μm from the GRIN lens. Figure 4(c) shows the measured beam profile at the focal plane and the full width half maximum (FWHM) is 4.4 μm. Figure 4(d) and (e) show the optical images of the aligned internal Lissajous scanning module with a PCB mounted MEMS scanner and the fully packaged handheld microscope catheter, respectively.

2.3. *Confocal microscopic imaging via handheld microscope catheter*

The fully packaged microscope catheter is finally coupled with a home-built confocal imaging system for real-time and *in vivo* confocal microscopic applications. Figure 5(a) shows the schematic illustration for confocal microscopic imaging based on handheld microscope catheter. Indocyanine green (ICG) fluorescence imaging was demonstrated by using a 785 nm fiber coupled laser source (LDM series 785, LASOS GmbH), coupled to FC/APC collimator and the laser excitation. The fluorescence emission signals are decoupled and filtered by using a dichroic

Biomedical Optics EXPRESS

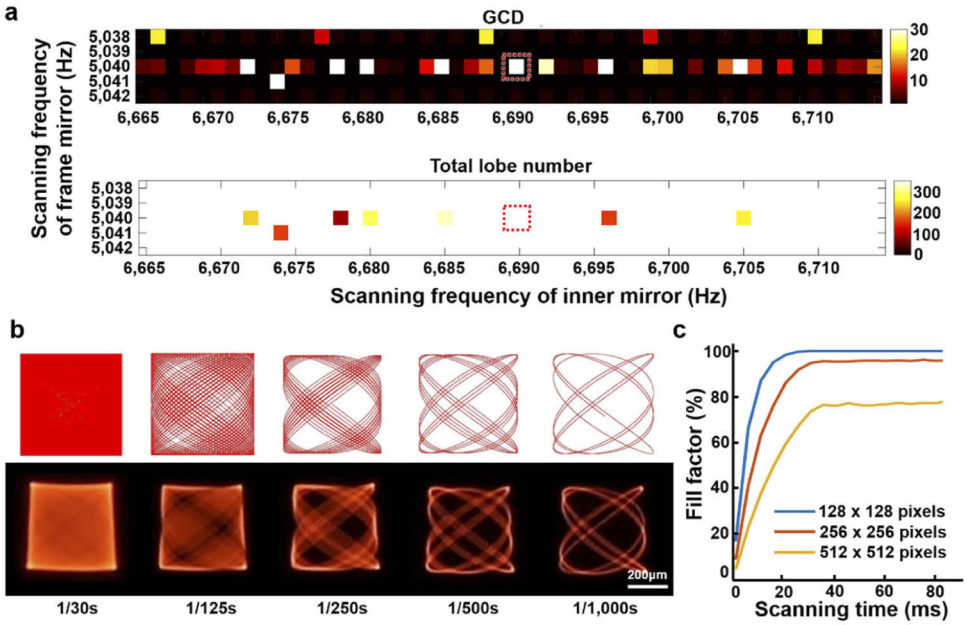

Fig. 3. a) Color maps of the GCD (top) and total lobe number (bottom) for selecting scanning frequencies along with the biaxial frequency domain. Scanning frequencies, which have GCD and total lobe numbers over 30 and 358, respectively, for 30 Hz frame rate and over 95% fill factor at 256×256 pixels. The selected frequencies are 5,040 Hz and 6,690 Hz and are represented in a dotted red box. The selected frequencies have GCD and the total lobe number equal to 30 and 391, respectively. b) The calculated trajectories at 256×256 pixels (top) and captured images of Lissajous patterns (bottom) with the selected frequency set along the scanning time. The Lissajous pattern fills the plane along the scanning time. c) A calculated fill factor along the scanning time at different pixel resolutions. The selected frequencies provide HDHF scanning with 95.4% fill factor at 1/30s at 256×256 pixels image.

mirror (FF801-Di02-25 × 36, Semrock, Inc.) and a bandpass filter (FF01-832/37-25, Semrock, Inc.), respectively. The measured total coupling efficiency of the system via the microscope catheter is 40%. Finally, the photomultiplier tube (R9110, Hamamatsu, Corp.) detects the fluorescence signals, which were received through an analog-to-digital converter of 8-M sampling clock. An image signal processor (ISP) reconstructs the confocal image of 256×256 pixels, based on the phase correction between the driving signal and detected signal [12]. In addition, the unscanned pixels are filled by applying a simple median filter. The reconstructed image is displayed on the monitor in real-time, i.e., 30 frames per sec.

Figure 5(b) shows the captured imaging result for the USAF resolution target. The first elements in group 7 corresponding to 3.9 μm line width are clearly resolved and the field of view (FOV) is 330 $\mu m \times 330$ μm. Figure 5(c) and (d) show versatile reflectance images of 330 μm × 330 μm in FOV, captured by the microscope catheter. Figure 5(e) shows the edge responses to a chrome line edge on a glass substrate at the center and periphery of the image, which are collected as the same condition as Fig. 5(b). The periphery of the image is slightly degraded due to the defocusing and the reduction of the cross-section area of the MEMS mirror along the tilting angle. A 10% to 90% transition width in the x-direction is 4.35 μm at both center and periphery of the image and thus the lateral resolution is 4.35 μm. Table 1 shows the detail

Biomedical Optics EXPRESS

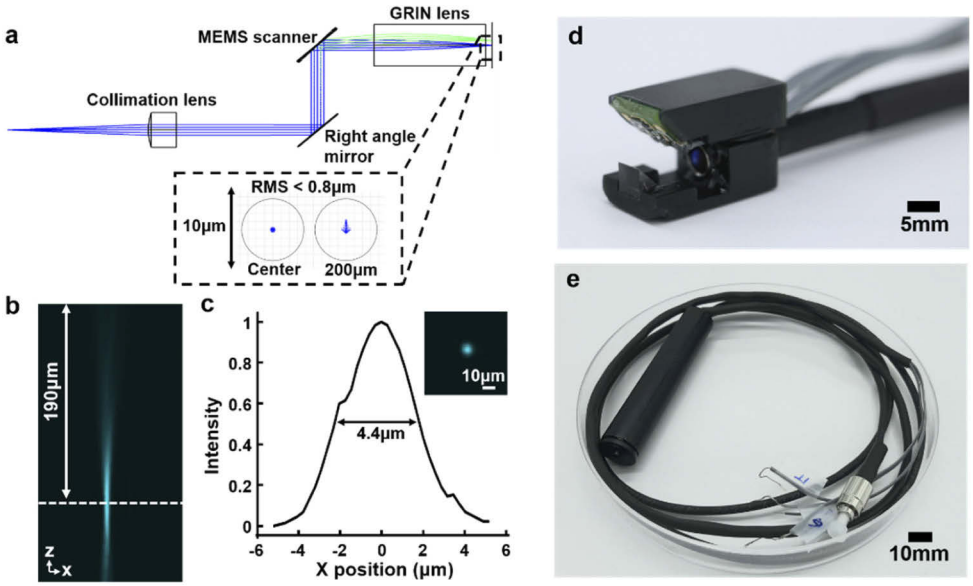

Fig. 4. a) The calculated spot diagrams at the center and the scanning amplitude of 200 μm on the focal plane. The circles represent an airy disk. b) The measured beam focusing through the fully packaged confocal microscope catheter. c) The beam profile at the focal plane. The working distance is about 190 μm from the GRIN lens, and the beam spot is 4.4 μm at the focus. Optical images of d) the Lissajous scanning module and e) the fully packaged handheld confocal microscope catheter.

specification of the entire system including the MEMS mirror, HDHF Lissajous scanning, and the confocal microscope catheter.

The confocal imaging system with a microscope catheter allows real-time *in vivo* and *ex vivo* mouse tissue imaging. The system uses 1 mW laser power for fluorescence imaging. Three 3-month-olds C57BL/6 mice were anesthetized by intraperitoneal injection of tribromoethanol (200 mg/kg) and 0.2 mL ICG (21980-100MG-F, Sigma Aldrich) solution (5 mg/mL; dissolved in phosphate buffer saline (PBS)) was intravenously injected via tail vein after 5 minutes. *In vivo* confocal imaging of capillaries on the toe was conducted in 5 minutes after ICG injection. Figure 6(a) and Visualization 1 show the experimental results. The high frame rate confocal imaging system overcomes motion artifact resulting from cardiac motion and microscope handling and thus clearly captures the capillaries during handheld operation. The ICG-injected mice were sacrificed under anesthesia for *ex vivo* tissue imaging for the liver, kidney, bladder, and lung. All the tissues were collected, gently washed in PBS after excision, and then subjected to *ex vivo* imaging. The system acquires the confocal images from ~ 50 μm depth of mouse tissue at 30 Hz frame rate and Fig. 6(b)-(e) shows the confocal images of the organs. The ICG molecules bind to plasma proteins in the blood [24] and stain the cytoplasm of organs, but not the nucleus. Therefore, the ICG stained areas and nuclei are captured as bright and dark areas, respectively, and it is clearly shown in the confocal image of the liver (Fig. 6(b)). The real-time confocal imaging system determines different morphologies of tissues such as glomerulus from the cross-section of the kidney (Fig. 6(c)), the detrusor muscle tissue of the bladder (Fig. 6(d)), and porous structure from pulmonary alveoli of the lung (Fig. 6(e)).

Biomedical Optics EXPRESS

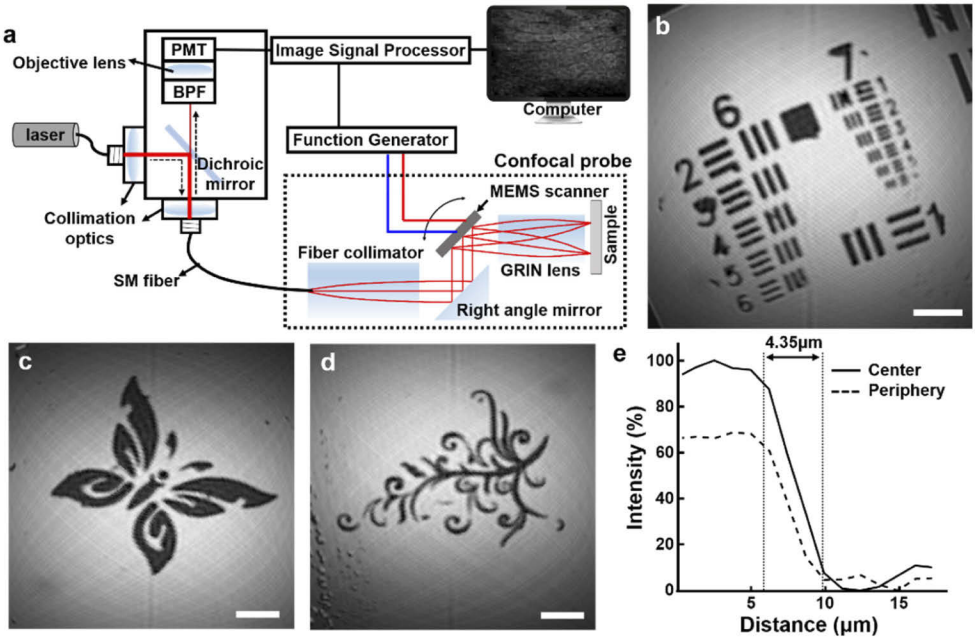

Fig. 5. a) Experimental set-up for a home-built confocal microscopic system coupled with hand-held microscope catheter. The confocal system reconstructs the confocal image of 256 × 256 pixels. Captured reflectance images of b) USAF resolution target and c, d) various metal patterns within 330 μm × 330 μm in FOV. The confocal system resolves the first elements in group 7, corresponding to 3.9 μm in line width. The scale bar indicates 50 μm. e) Edge response to a chrome line edge on a glass substrate at the center and periphery of the image.

Table 1. Specifications of the MEMS mirror, HDHF Lissajous scanning and the confocal microscope catheter.

	HDHF Lissajous scanning mirror	
	Frame mirror	Inner mirror
Resonant frequency	5,038 Hz	6,665 Hz
Q-factor	201.9	60.5
Scanning angle	6.5°	13°
Driving voltage	34 Vpp	22 Vpp
	HDHF Lissajous scanning	
Scanning frequency	5,040 Hz (Frame mirror) / 6,690 Hz (Inner mirror)	
Pixel resolution	256 × 256 pixels	
Frame rate	30 Hz	
Fill factor	95.4%	
	Confocal microscope catheter	
Lateral resolution	4.35 μm	
FOV	330 μm x 330 μm	

Biomedical Optics EXPRESS

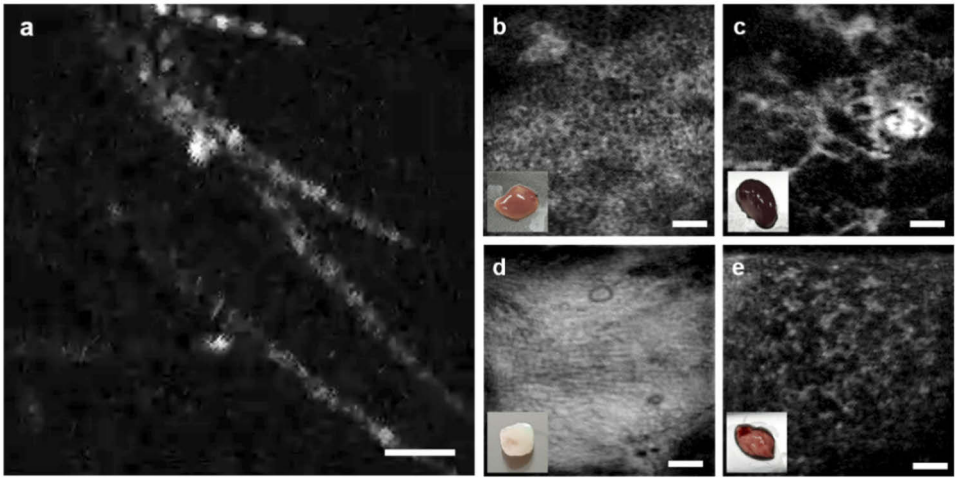

Fig. 6. a) *In vivo* imaging result of capillaries on the toe, and *ex vivo* imaging result of the b) liver, c) kidney, d) bladder, e) lung of the mouse. All confocal images were acquired at 30 Hz frame rate and 256×256 pixels image. The scale bars indicate 50 μm.

3. Conclusion

In summary, we have successfully demonstrated the real-time and handheld confocal microscope for real-time, *in vivo* and ex vivo tissue imaging by using HDHF Lissajous scanning MEMS mirror. The compact laser scanning microscope catheter including optical components for beam collimation and reflection, the scanning MEMS mirror, and a GRIN lens, was fully packaged and coupled with a home-built confocal imaging system. The selected scanning frequencies for HDHF Lissajous scanning are 5,040 Hz and 6,690 Hz, which provide 30 Hz frame rate and 95.4% fill factor for 256×256 pixels. The measured lateral resolution is 4.35 μm for 330 μm x 330 μm in FOV. Finally, real-time *in vivo* and *ex vivo* confocal imaging of mouse tissues have been successfully demonstrated at 30 Hz frame rate, using the handheld confocal microscope catheter. This real-time handheld confocal microscopic system can provide diverse *in vivo* and *ex vivo* cellular applications for advanced optical biopsy.

Funding. National Research Foundation of Korea (2021R1A2B5B03002428, NRF-2021R1C1C1011567); Ministry of Trade, Industry and Energy (P0013915).

Acknowledgements. This work was supported by the National Research Foundation of Korea (NRF) funded by the Ministry of Science ICT & Future Planning (2021R1A2B5B03002428, NRF-2021R1C1C1011567) and Ministry of Trade, Industry & Energy, Republic of Korea (P0013915).

Disclosures. The authors declare no conflicts of interest.

Data availability. Data underlying the results presented in this paper are not publicly available at this time but may be obtained from the authors upon request.

References

1. M. Slaoui and L. Fiette, "Histopathology procedures: from tissue sampling to histopathological evaluation," *Drug Safety Evaluation* (Humana Press, 2011), pp. 69–82.
2. E. S. Flores, M. Cordova, K. Kose, W. Phillips, A. Rossi, K. Nehal, and M. Rajadhyaksha, "Intraoperative imaging during Mohs surgery with reflectance confocal microscopy: initial clinical experience," J. Biomed. Opt. **20**(6), 061103 (2015).
3. P. Kim, M. Pouris' haag, D. Côté, C. P. Lin, and S.-H. Yun, "In vivo confocal and multiphoton microendoscopy," J. Biomed. Opt. **13**(1), 010501 (2008).
4. S. Lee, C. Vinegoni, M. Sebas, and R. Weissleder, "Automated motion artifact removal for intravital microscopy, without a priori information," Sci. Rep. **4**(1), 4507 (2015).

Biomedical Optics EXPRESS

5. H. C. Park, C. Song, M. Kang, Y. Jeong, and K. H. Jeong, "Forward imaging OCT endoscopic catheter based on MEMS lens scanning," Opt. Lett. **37**(13), 2673–2675 (2012).
6. C. L. Arrasmith, D. L. Dickensheets, and A. Mahadevan-Jansen, "MEMS-based handheld confocal microscope for in-vivo skin imaging," Opt. Express **18**(4), 3805–3819 (2010).
7. X. Duan, H. Li, Z. Qiu, B. P. Joshi, A. Pant, A. Smith, K. Kurabayashi, K. R. Oldham, and T. D. Wang, "MEMS-based multiphoton endomicroscope for repetitive imaging of mouse colon," Biomed. Opt. Express **6**(8), 3074–3083 (2015).
8. Y. Wang, M. Raj, H. S. McGuff, G. Bhave, B. Yang, T. Shen, and X. Zhang, "Portable oral cancer detection using a miniature confocal imaging probe with a large field of view," J. Micromech. Microeng. **22**(6), 065001 (2012).
9. C. Y. Yao, B. Li, and Z. Qiu, "2D Au-coated resonant MEMS scanner for NIR fluorescence intraoperative confocal microscope," Micromachines **10**(5), 295 (2019).
10. D. R. Rivera, C. M. Brown, D. G. Ouzounov, I. Pavlova, D. Kobat, W. W. Webb, and C. Xu, "Compact and flexible raster scanning multiphoton endoscope capable of imaging unstained tissue," Proc. Natl. Acad. Sci. **108**(43), 17598–17603 (2011).
11. H. Schulz-Hildebrandt, T. Pfeiffer, T. Eixmann, S. Lohmann, M. Ahrens, J. Rehra, W. Draxinger, P. König, R. Huber, and G. Hüttmann, "High-speed fiber scanning endoscope for volumetric multi-megahertz optical coherence tomography," Opt. Lett. **43**(18), 4386–4389 (2018).
12. K. Hwang, Y. Seo, D. Y. Kim, J. Ahn, S. Lee, K. H. Han, K. H. Lee, S. Jon, P. Kim, K. E. Yu, H. Kim, S. H. Kang, and K. H. Jeong, "Handheld endomicroscope using a fiber-optic harmonograph enables real-time and in vivo confocal imaging of living cell morphology and capillary perfusion," Microsyst. Nanoeng. **6**(1), 72 (2020).
13. J. M. Jabbour, M. A. Saldua, J. N. Bixler, and K. C. Maitland, "Confocal endomicroscopy: instrumentation and medical applications," Ann. Biomed. Eng. **40**(2), 378–397 (2012).
14. J. T. Liu, M. J. Mandella, N. O. Loewke, H. Haeberle, H. Ra, W. Piyawattanametha, O. D. Solgaard, G. S. Kino, and C. H. Contag, "Micromirror-scanned dual-axis confocal microscope utilizing a gradient-index relay lens for image guidance during brain surgery," J. Biomed. Opt. **15**(2), 026029 (2010).
15. C. Yin, A. K. Glaser, S. Y. Leigh, Y. Chen, L. Wei, P. C. S. Pillai, M. C. Rosenberg, S. Abeytunge, G. Peterson, C. Glazowski, N. Sanai, M. J. Mandella, M. Rajadhyaksha, and J. T. C. Liu, "Miniature in vivo MEMS-based line-scanned dual-axis confocal microscope for point-of-care pathology," Biomed. Opt. Express **7**(2), 251–263 (2016).
16. L. Wei, C. Yin, Y. Fujita, N. Sanai, and J. T. Liu, "Handheld line-scanned dual-axis confocal microscope with pistoned MEMS actuation for flat-field fluorescence imaging," Opt. Lett. **44**(3), 671–674 (2019).
17. Q. A. Tanguy, O. Gaiffe, N. Passilly, J. M. Cote, G. Cabodevila, S. Bargiel, P. Lutz, H. Xie, and C. Gorecki, "Real-time Lissajous imaging with a low-voltage 2-axis MEMS scanner based on electrothermal actuation," Opt. Express **28**(6), 8512–8527 (2020).
18. S. Z. Sullivan, R. D. Muir, J. A. Newman, M. S. Carlsen, S. Sreehari, C. Doerge, N. J. Begue, R. M. Everly, C. A. Bouman, and G. J. Simpson, "High frame-rate multichannel beam-scanning microscopy based on Lissajous trajectories," Opt. Express **22**(20), 24224–24234 (2014).
19. K. Hwang, Y. H. Seo, J. Ahn, P. Kim, and K. H. Jeong, "Frequency selection rule for high definition and high frame rate Lissajous scanning," Sci. Rep. **7**(1), 1–8 (2017).
20. Y. H. Seo, K. Hwang, H. Kim, and K. H. Jeong, "Scanning MEMS mirror for high definition and high frame rate lissajous patterns," Micromachines **10**(1), 67 (2019).
21. J. H. Lee, S. T. Lee, C. M. Yao, and W. Fang, "Comments on the size effect on the microcantilever quality factor in free air space," J. Micromech. Microeng. **17**(1), 139–146 (2007).
22. Y. S. Chiu, K. S. Chang, R. W. Johnstone, and M. Parameswaran, "Fusetethers in MEMS," J. Micromech. Microeng. **3**, 1525–1528 (2006).
23. W. Shahid, Z. Qiu, X. Duan, H. Li, T. D. Wang, and K. R. Oldham, "Modeling and simulation of a parametrically resonant micromirror with duty-cycled excitation," J. Microelectromech. Syst. **23**(6), 1440–1453 (2014).
24. S. Yoneya, T. Saito, Y. Komatsu, I. Koyama, K. Takahashi, and J. Duvoll-Young, "Binding properties of indocyanine green in human blood," Invest. Ophthalmol. Visual Sci. **39**(7), 1286–1290 (1998).